Field-dependent dynamic responses from dilute magnetic nanoparticle dispersions

Jeppe Fock,[a] Christoph Balceris,[b] Rocio Costo,[c] Lunjie Zeng,[d] Frank Ludwig,[b] and Mikkel Fougt Hansen*[a]

Supplementary information

S1 Langevin dynamics

This section describes the theory and results of stochastic simulations (Langevin dynamics) performed to validate and compare to the results of the Fokker-Planck simulations.

To calculate the dynamic response, the torque (Eq. (11)) is equated to the viscous drag torque $-f_r\Omega$, where Ω is the angular velocity of the particle rotation and f_r is the rotational friction coefficient, and a stochastic term is included in the expression as

$$f_r\Omega = \tau + \sqrt{2k_BTf_r}\mathscr{H}, \tag{S1}$$

where the inertia of the particle has been neglected. The rotational friction coefficient is related to the Brownian relaxation time as

$$\tau_B = \frac{f_r}{2k_BT} \tag{S2}$$

Due to the assumption of prolate particles, the rotation around the major axis (caused by random forces) does not affect the properties of the dispersion (absorption/magnetisation). As a consequence and to simplify the treatment, the inertia of rotation around the major axis can be assumed to be equal to the inertia of rotation around the minor axis. The rotational friction coefficient for rotation of a prolate ellipsoid particle around the equatorial semiaxes is given by

$$f_r = \frac{2\pi}{3}\,\frac{\eta D_h^3}{p_c^2}\,\frac{(1/p_c)^2-(p_c)^2}{1-S[2-(1/p_c)^2]} \tag{S3}$$

where η is the dynamic fluid viscosity, $S = \tanh^{-1}(\xi)/\xi$ and $\xi = \sqrt{p^2-1}/p$. p_c is the aspect ratio, calculated as the ratio between major axis (diameter p_cD_h) and the minor axis (diameter D_h).[1] For a sphere ($p_c = 1$), the rotational friction coefficient reduces to $\pi\eta D_h^3$.

The last term in Eq. (S1) accounts for random forces. k_B is Boltzmann's constant. $\mathscr{H}$ is a white noise force, which can be approximated numerically by a vector of Gaussian distributed random numbers with zero mean and unit standard deviation $\mathbf{W}$ scaled by $\sqrt{\Delta t}$.[2]

Using $\mathrm{d}\mathbf{e}/\mathrm{d}t = \Omega\times\mathbf{e}$ and $\mathbf{H} = H\mathbf{n}$, the change in the particle orientation of the particle can be found as

$$\frac{\Delta\mathbf{e}}{\Delta t} = \frac{1}{2\tau_B}\left[(\beta_0+\gamma_0\mathbf{e}\cdot\mathbf{n})(\mathbf{e}\times\mathbf{n}\times\mathbf{e}) - 2\mathbf{e}\right] + \left(\frac{1}{\tau_B\Delta t}\right)^{\frac{1}{2}}\mathbf{W}\times\mathbf{e} \tag{S4}$$

where the last term in the square bracket ensures convergence to Boltzmann equilibrium and conversion of magnetisation when transformed from the Stratonovitch to the Ito calculus.[3–5]

All simulations below were performed for ensembles of $2\cdot10^4$ magnetic nanoparticles (MNPs) with a diameter of 100 nm dispersed in water at room temperature ($T = 295\,\mathrm{K}$, $\eta = 1\,\mathrm{mPa\,s}$).

S1.1 Validation of stochastic simulations

To test the validity of the stochastic simulations, we first simulated the demagnetisation of MNPs, all initially pointed along the z-direction, using a time step of $\Delta t = 3\,\mu\mathrm{s}$. The result is shown in Fig. S1a along with the theoretically expected

[a] Department of Micro- and Nanotechnology, DTU Nanotech, Bldg. 345B, Technical University of Denmark, DK-2800 Kongens Lyngby, Denmark, Email: jepf@nanotech.dtu.dk, Mikkel.Hansen@nanotech.dtu.dk
[b] Institute of Electrical Measurement and Fundamental Electrical Engineering, Technische Universität Braunschweig, Braunschweig D-38106, Germany
[c] Instituto de Ciencia de Materiales de Madrid, ICMM/CSIC, Sor Juana Ines de la Cruz 3, 28049 Madrid, Spain
[d] Department of Physics, Chalmers University of Technology, Gothenburg 41296, Sweden

exponential decay, $M(t) = M(0)\exp(-t/\tau_B)$, with

$$\tau_B = \frac{3\eta V_h}{k_B T}. \tag{S5}$$

The simulation results were found to agree with the theoretical expectation within 1 %. This agreement could be further improved by increasing the number of particles in the simulation.

We further verified that the equilibrium value of the magnetisation agreed with that expected from Boltzmann statistics (the Langevin function) at a number of fields and temperatures. Fig. S1b shows the simulation results as well as the Langevin function. Again, the stochastic simulation results were found to agree with the Langevin function within 1 %, concurring with the findings of Reeves and Weaver.[2] This demonstrates the validity of the employed numerical scheme to calculate the correct dynamic and equilibrium response of MNPs with a permanent magnetic moment.

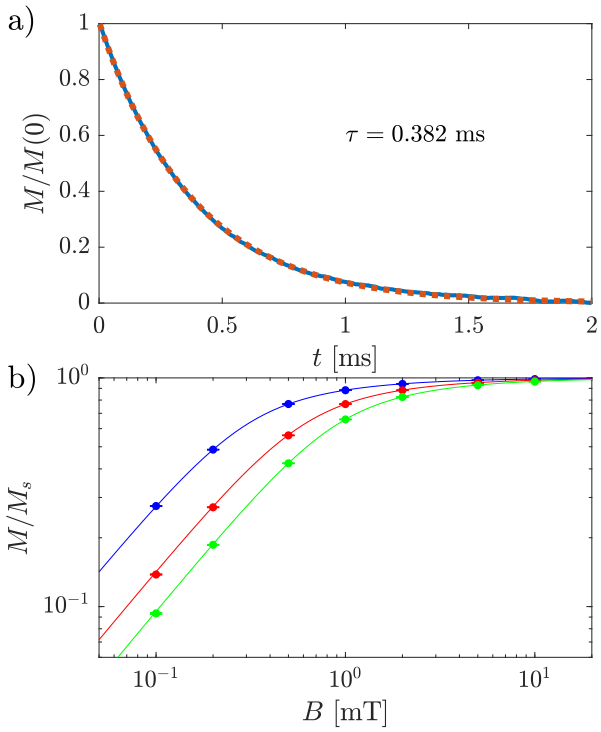

Fig. S1 (a) Demagnetisation of $2 \cdot 10^4$ particles all initially pointing in the z direction. In the figure the fitted value of the exponential decay ($M(t) = M(0)\exp(-t/\tau_B)$ is shown. (b) Magnetisation of $2 \cdot 10^4$ random oriented particles at 300 K (green) 200 K (red) and 100 K (blue). Points indicate the simulation results obtained at time $t = 9\tau_B$, solid lines are the Langevin function.[2]

S1.2 Comparison of stochastic simulations and Fokker-Planck simulations

Figure S2 compares the results for the AC susceptibility and the optomagnetic data obtained using stochastic simulations and Fokker-Planck simulations. A good agreement between the methods is obtained both for low and high values of β_0 and γ_0.

For the stochastic simulations, the signal has to be averaged over many particles or periods to obtain a signal with low noise. The Fokker-Planck simulation is insensitive to signal noise and consequently provides good results also for very low γ_0 and β_0 values. On the other hand, for large values of γ_0 or β_0 the Fokker-Planck simulations have to be truncated at high values of l and p for the problem to converge, and consequently the calculation takes longer time.

S2 Derivation of Fokker-Planck system of linear equations

In this section the details of the derivations of the Fokker-Planck results are shown. We have used $f_B = 1/(2\pi\tau_B)$ in the calculations.

First, defining $x = \cos\theta$, Eq. (16) is simplified to

$$\frac{\partial f}{\partial t} = \frac{1}{2\tau_B}\frac{\partial}{\partial x}\left[(1-x^2)\left(\frac{\partial f}{\partial x} - (\beta_0 \cos\omega t + x\gamma_0 \cos^2\omega t) f\right)\right] \tag{S6}$$

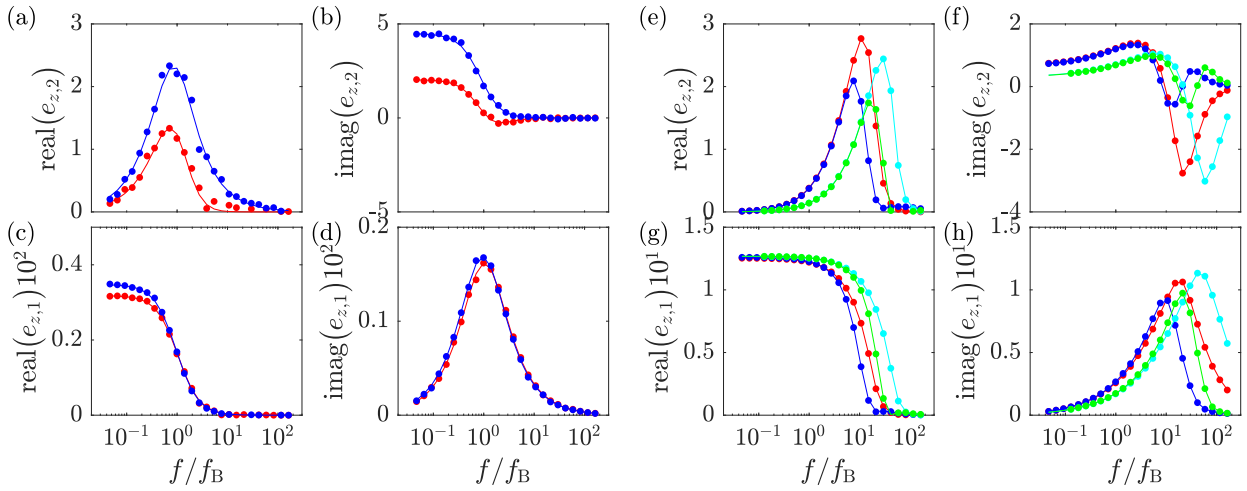

Fig. S2 Dynamic simulations (points) using 10^4 particles compared to Fokker-Planck simulations (solid lines). (a)-(d) red ($\beta_0 = 1$, $\gamma_0 = 0$); blue ($\beta_0 = 1$, $\gamma_0 = 1$). (e)-(h) red ($\beta_0 = 100$, $\gamma_0 = 0$), blue ($\beta_0 = 100$, $\gamma_0 = 100$), cyan ($\beta_0 = 300$, $\gamma_0 = 0$), and green ($\beta_0 = 300$, $\gamma_0 = 300$).

Using the orthogonality of the Legendre polynomials and that $P_0 = 1$, the normalisation of $f(x,t)$ gives

$$\int_{-1}^{1} f(x,t)\mathrm{d}t = \sum_{p=0}^{\infty}\Big(A_{0,p}\cos p\omega t + B_{0,p}\sin p\omega t\Big)2 = 1 \tag{S7}$$

Thus, $A_{0,p} = B_{0,p} = 0$, except for $A_{0,0} = \frac{1}{2}$, to ensure that $f(x,t)$ is normalised for all t.

Inserting $f(x,t)$ in Eq. (S6) we obtain

$$\frac{\partial f}{\partial t} = \frac{1}{2\tau_B}\sum_{l=0} C_l(t)\frac{\partial}{\partial x}\left[(1-x^2)\left(\frac{\partial P_l(x)}{\partial x} - (\beta_0\cos\omega t + x\gamma_0\cos^2\omega t)P_l(x)\right)\right]. \tag{S8}$$

where the x dependence of the Legendre polynomials is implicit, i.e, $P_l = P_l(x)$.

We consider the three terms separately and use the properties of the Legendre polynomials*

$$\frac{\partial}{\partial x}\left[(1-x^2)\frac{\partial P_l}{\partial x}\right] = -l(l+1)P_l \tag{S9}$$

$$\begin{aligned}\frac{\partial}{\partial x}\left[(1-x^2)P_l\right] &= \frac{1}{2l+1}\frac{\partial}{\partial x}\left[(1-x^2)\frac{\partial}{\partial x}\Big(P_{l+1}-P_{l-1}\Big)\right]\\ &= \frac{1}{2l+1}\Big[-(l+1)(l+2)P_{l+1} + l(l-1)P_{l-1}\Big]\end{aligned} \tag{S10}$$

$$\begin{aligned}\frac{\partial}{\partial x}\left[(1-x^2)xP_l\right] &= \frac{1}{2l+1}\frac{\partial}{\partial x}\left[(1-x^2)\Big((l+1)P_{l+1} + lP_{l-1}\Big)\right]\\ &= \frac{1}{2l+1}\frac{\partial}{\partial x}\left[(1-x^2)\frac{\partial}{\partial x}\left(\frac{l+1}{2l+3}(P_{l+2}-P_l) + \frac{l}{2l-1}(P_l - P_{l-2})\right)\right]\\ &= \frac{1}{2l+1}\left(\frac{l+1}{2l+3}(-(l+2)(l+3)P_{l+2} + l(l+1)P_l) + \frac{l}{2l-1}(-l(l+1)P_l + (l-2)(l-1)P_{l-2})\right)\\ &= -\frac{(l+1)(l+2)(l+3)}{(2l+1)(2l+3)}P_{l+2} - \frac{(l+1)l}{(2l+3)(2l-1)}P_l + \frac{(l-2)(l-1)l}{(2l+1)(2l-1)}P_{l-2}\end{aligned} \tag{S11}$$

* From the Legendre differential equation, $\frac{\mathrm{d}}{\mathrm{d}x}\left[(1-x^2)\frac{\mathrm{d}}{\mathrm{d}x}P_l(x)\right] = -l(l+1)P_l(x)$, and the properties of differentiation, $P_l(x) = \frac{1}{2l+1}\frac{\mathrm{d}}{\mathrm{d}x}\left[P_{l+1}(x) - P_{l-1}(x)\right]$

Using the orthogonality of the Legendre polynomials, Eq. (S8) becomes

$$\frac{\partial C_l(t)}{\partial t} = \frac{l(l+1)}{2\tau_B}\Bigg[-C_l(t) + \beta_0 \cos\omega t\left(\frac{1}{2l-1}C_{l-1}(t) - \frac{1}{2l+3}C_{l+1}(t)\right) + \gamma_0 \cos^2\omega t\left(\frac{(l-1)}{(2l-3)(2l-1)}C_{l-2}(t) + \frac{1}{(2l+3)(2l-1)}C_l(t) - \frac{(l+2)}{(2l+5)(2l+3)}C_{l+2}\right)\Bigg] \tag{S12}$$

From Eq. (S8) we also need to evaluate $C_l(t)\cos\omega t$ and $C_l(t)\cos^2\omega t$

$$C_l(t)\cos\omega t = \frac{1}{2}\sum_{p=0}^{\infty} A_{l,p}\big(\cos(p-1)\omega t + \cos(p+1)\omega t\big) + B_{l,p}\big(\sin(p-1)\omega t + \sin(p+1)\omega t\big) \tag{S13}$$

$$C_l(t)\cos^2\omega t = \frac{1}{4}\sum_{p=0}^{\infty} A_{l,p}\big(2\cos p\omega t + \cos(p-2)\omega t + \cos(p+2)\omega t\big) + B_{l,p}\big(2\sin p\omega t \sin(p-2)\omega t + \sin(p+2)\omega t\big) \tag{S14}$$

Using Eqs. (S12), (S13) and (S14) we can write Eq. (S8) as a system of linear equations as

$$\begin{aligned} n\omega B_{l,p} = \frac{l(l+1)}{2\tau_B}\Bigg[& -A_{l,p} + \frac{\beta_0}{2}\Bigg(\frac{1}{2l-1}\big((1+\delta_{p,1})A_{l-1,p-1} + A_{l-1,p+1}\big) - \\ & \frac{1}{2l+3}\big((1+\delta_{p,1})A_{l+1,p-1} + A_{l+1,p+1}\big)\Bigg) + \\ & \frac{\gamma_0}{4}\Bigg(\frac{(l-1)}{(2l-3)(2l-1)}\big((2+\delta_{p,1})A_{l-2,p} + (1+\delta_{p,2})A_{l-2,p-2} + A_{l-2,p+2}\big) + \\ & \frac{1}{(2l+3)(2l-1)}\big((2+\delta_{p,1})A_{l,p} + (1+\delta_{p,2})A_{l,p-2} + A_{l,p+2}\big) - \\ & \frac{(l+2)}{(2l+5)(2l+3)}\big((2+\delta_{p,1})A_{l+2,p} + (1+\delta_{p,2})A_{l+2,p-2} + A_{l+2,p+2}\big)\Bigg)\Bigg] \end{aligned} \tag{S15}$$

$$\begin{aligned} -n\omega A_{l,p} = \frac{l(l+1)}{2\tau_B}\Bigg[& -B_{l,p} + \frac{\beta_0}{2}\Bigg(\frac{1}{2l-1}\big(B_{l-1,p-1} + B_{l-1,p+1}\big) - \\ & \frac{1}{2l+3}\big(B_{l+1,p-1} + B_{l+1,p+1}\big)\Bigg) + \\ & \frac{\gamma_0}{4}\Bigg(\frac{(l-1)}{(2l-3)(2l-1)}\big((2-\delta_{p,1})B_{l-2,p} + B_{l-2,p-2} + B_{l-2,p+2}\big) + \\ & \frac{1}{(2l+3)(2l-1)}\big((2-\delta_{p,1})B_{l,p} + B_{l,p-2} + B_{l,p+2}\big) - \\ & \frac{(l+2)}{(2l+5)(2l+3)}\big((2-\delta_{p,1})B_{l+2,p} + B_{l+2,p-2} + B_{l+2,p+2}\big)\Bigg)\Bigg] \end{aligned} \tag{S16}$$

In the above equations $\delta_{j,k}$ denotes the Kronecker delta function where $\delta_{j,k} = 1$ if $j = k$ and $\delta_{j,k} = 0$ otherwise. The equations contain only either even or odd values of $l + p$. Thus, the even and odd sets of variables are decoupled. Further, because the only inhomogeneous term, $A_{0,0}$, is even only the even values of $l + p$ are non-zero. To calculate the second moment we need to express x^2 in terms of Legendre polynomials as

$$x^2 = \frac{2}{3}P_2(x) + \frac{1}{3}P_0(x). \tag{S17}$$

Then, the second moment is

$$\overline{e_z^2} = \int_{-1}^{1} x^2 f(x,t)\mathrm{d}x = \int_{-1}^{1} \left(\frac{2}{3}P_2(x) + \frac{1}{3}P_0(x)\right) f(x,t)\mathrm{d}x \tag{S18}$$

$$= \sum_{p=0}^{\infty} \frac{4}{15}\left(A_{2,p}\cos p\omega t + B_{2,n}\sin p\omega t\right) + \frac{2}{3}\left(A_{0,p}\cos p\omega t + B_{0,p}\sin p\omega t\right) \tag{S19}$$

$$= \frac{4}{15}\sum_{p=0}^{\infty}\left(A_{2,p}\cos p\omega t + B_{2,p}\sin p\omega t\right) + \frac{1}{3} \tag{S20}$$

Writing in complex notation, the p'th harmonics become

$$\overline{e_z}_{,p} = \frac{2}{3}\left(A_{1,p} + \mathrm{i}B_{1,p}\right) \tag{S21}$$

$$\overline{e_z^2}_{,p} = \frac{4}{15}\left(A_{2,p} + \mathrm{i}B_{2,p}\right) \quad \text{for } p > 0 \tag{S22}$$

$$\overline{e_z^2}_{,0} = \frac{1}{3} + \frac{4}{15}A_{2,0} \tag{S23}$$

and the Fourier transform becomes

$$\overline{e_z}(p\omega) = \left(\frac{\pi}{2}\right)^{1/2}\overline{e_z}_{,p} \tag{S24}$$

$$\overline{e_z^2}(p\omega) = \left(\frac{\pi}{2}\right)^{1/2}\overline{e_z^2}_{,p} \quad \text{for } p > 0 \tag{S25}$$

$$\overline{e_z^2}(0) = (2\pi)^{1/2}\overline{e_z^2}_{,0} \tag{S26}$$

S2.1 Frequency domain representation of signals

The magnetic susceptibility and optomagnetic signals can be expressed in the frequency domain. First, the Fourier transforms of $M(t)$ and $V(t)$ for $H(t) = H_0\cos\omega t$ are found:

$$\frac{M(\omega')}{n} = \chi V H_0\left[\frac{\widetilde{K}}{2}\left(\frac{2}{\pi}\right)^{1/2}\left(\overline{e_z^2}(\omega'+\omega) + \overline{e_z^2}(\omega'-\omega)\right) + \frac{\delta(\omega'+\omega)+\delta(\omega'-\omega)}{1+\chi N_\perp}\right]$$

$$+ m\left(\frac{2}{\pi}\right)^{1/2}\overline{e_z}(\omega') \tag{S27}$$

$$\frac{V(\omega')}{V_{\mathrm{ref}}} = \sqrt{2\pi}\delta(\omega')\left(1 + \frac{1}{3}nz\Delta\sigma\right) - nz\Delta\sigma\left(\frac{2}{\pi}\right)^{1/2}\overline{e_z^2}(\omega') \tag{S28}$$

Then, the first harmonic of the magnetic signal, M_1, and the second harmonic of the optomagnetic signal, V_2 are found and expressed in terms of the p'th harmonics of $\overline{e_z}$ and $\overline{e_z^2}$ as

$$\frac{M_1}{n} = \chi V_c H_0\left[\frac{\widetilde{K}}{2}\left(\overline{e_z^2}_{,2} + 2\overline{e_z^2}_{,0}\right) + \frac{1}{1+\chi N_\perp}\right] + m\overline{e_z}_{,1} \tag{S29}$$

$$\chi_1 = 3\chi_0\left[\frac{1}{\beta_0}\overline{e_z}_{,1} + \frac{\alpha}{2}\left(\overline{e_z^2}_{,2} + 2\overline{e_z^2}_{,0}\right)\right] + \frac{n\chi V_c}{1+\chi N_\perp} \tag{S30}$$

$$\frac{V_2}{V_{\mathrm{ref}}} = -nz\Delta\sigma\overline{e_z^2}_{,2} \tag{S31}$$

with $\chi_0 = n\mu_0 m^2/(3k_{\mathrm{B}}T)$.

Note, that in our previous work (and also in this work), experimental results are reported for a sine reference applied magnetic field rather than the cosine reference field used in the derivation of the Fokker-Planck equation. The second harmonic signal for a cosine reference, $\tilde{V}_2 = \tilde{V}_2' - \mathrm{i}\tilde{V}_2''$, is related to the second harmonic signal obtained for a sine reference,

$V_2 \equiv V_2' + \mathrm{i}V_2''$, as $\tilde{V}_2' = -V_2''$ and $\tilde{V}_2'' = -V_2'$.[6]

S3 Fit of low-β_0 spectra

The low-β_0 ($\beta_0 = 10^{-3}$) optomagnetic and magnetic spectra calculated using Fokker-Planck simulations with no induced magnetic moment are shown in Fig. S3a-d. The Fokker-Planck simulation results were compared to the low-field approximations given by the Debye model, $\chi_1 = (1 + \mathrm{i}f/f_\mathrm{B})^{-1}$, for the magnetic AC susceptibility and by $\mathrm{i}\chi_1^2$ for the optomagnetic signal.

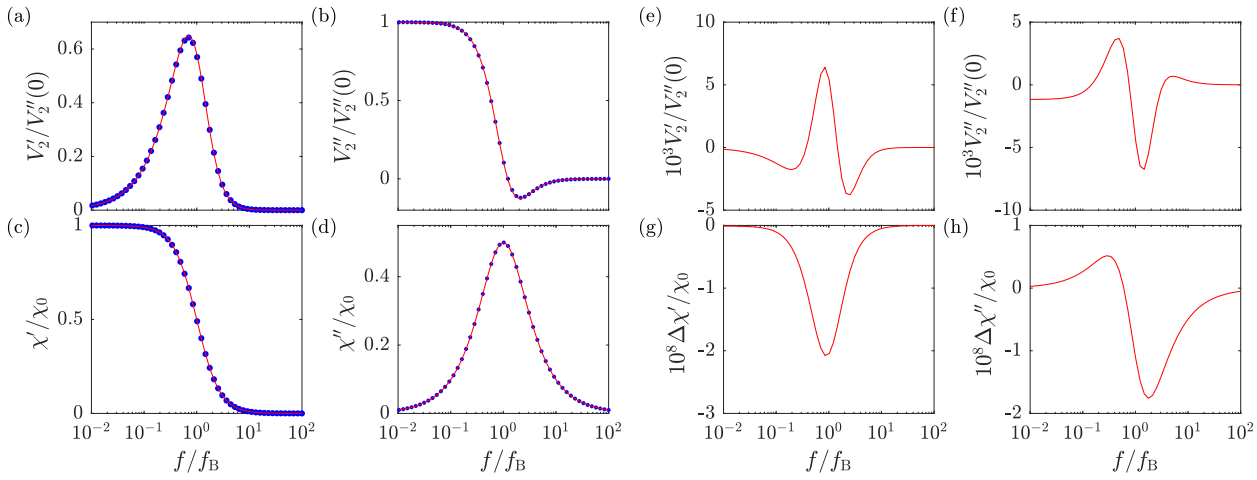

Fig. S3 (a)-(d) Fokker-Planck simulation results obtained for (blue dots) with $\beta_0 = 0.001$ and $\gamma_0 = 0$ and analytical low-field model (red line) fits. Panels (a) and (b) show V_2' and V_2'' normalised by the low-frequency amplitude. Panels (c) and (d) show χ_1' and χ_1'' normalised by the low-frequency amplitude, $\chi_1'(0)$. Panels (e)-(h) show the residuals from the fits in panels (a)-(d).

The Debye model provides a precise description of the low-field magnetic susceptibility signal; the residuals (Fig. S3g-h) are very small and are further decreased when reducing β_0. To fit the optomagnetic signal, however, the analytical model had to be modified. By shifting the Brownian relaxation frequency, a reasonable fit was obtained to

$$V_2 = \mathrm{i}\left(\frac{1}{1 + \mathrm{i}\frac{f}{1.21 f_\mathrm{B}}}\right)^2. \tag{S32}$$

The residuals (Fig. S3e-f), show a systematic deviation, which is not further reduced when reducing β_0. This indicates that the low-field model ($\mathrm{i}\chi_1^2$) does not provide an accurate description of the low-field OM signal. It is noted, however, that the deviation from the correct line shape is less than about 1% of the low-frequency signal level.

S4 New ACS approximation

Fig. S4 and Fig. S5 compares the analytical approximations developed by Yoshida and Enpuku and in this work to results from Fokker-Planck simulations.

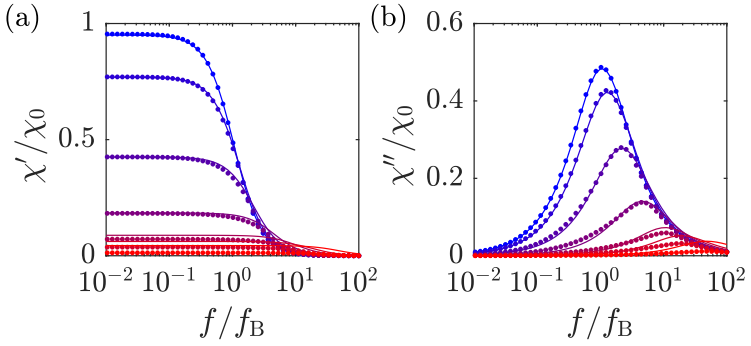

Fig. S4 Comparison between analytical model by Yoshida and Enpuku[7] (lines) and Fokker-Planck calculations with $\alpha = 0$ (points) for $\beta_0 = 0.99, 2.7, 7.2, 19, 52, 102, 300$ (blue to red).

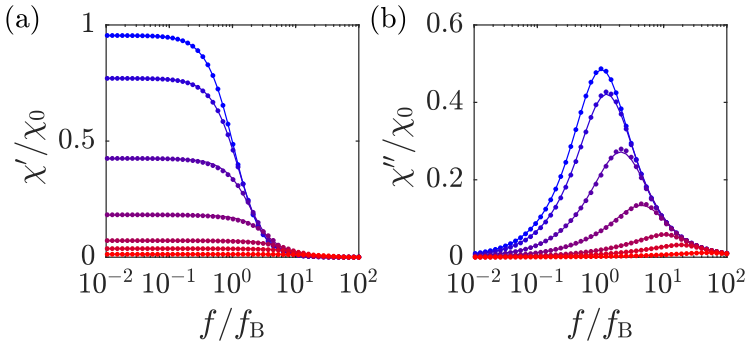

Fig. S5 Comparison between improved analytical approximation of the ACS signal, Eqs. (46)-(53) (lines) and Fokker-Planck calculations with $\alpha = 0$ (points) for $\beta_0 = 0.99, 2.7, 7.2, 19, 52, 102, 300$ (blue to red).

S5 Analytical OM approximation

The magnetic field- and frequency-dependent optomagnetic signal for zero induced magnetic moment ($\chi = 0$) can to a good approximation be described by

$$\frac{V_2'}{V_2''(0)} = \frac{2^a k \left(\frac{f}{f_{\mathrm{B1}}}\right)^b}{\left(\left(\frac{f}{f_{\mathrm{B1}}}\right)^c + 1\right)^{2a}} \tag{S33}$$

$$\frac{V_2''}{V_2''(0)} = \frac{\left(1 - \frac{f^2}{f_0^2}\right)}{\left(\left(\frac{f}{f_{\mathrm{B2}}}\right)^h + 1\right)^{2d}} \left(\frac{f}{f_{\mathrm{B3}}} + 1\right)^g \left(\frac{\left(\frac{f}{f_0} + 1\right)^2}{\left(\frac{f}{f_{\mathrm{B4}}} + 1\right)^2}\right)^j \tag{S34}$$

where $V_2''(0)$ is the equilibrium response calculated by Fock *et al.*[6] or alternatively given by

$$V_2''(0) = \frac{{\beta_0}^2}{45\left(0.1051\,{\beta_0}^{1.8036} - 0.0156\,\beta_0 + 0.007298\,{\beta_0}^{2.7939} + 1.0\right)^{0.99666}} \tag{S35}$$

with the parameters

$$f_0 = 1.22475 f_B \left(1 + 0.0511 \beta_0^{1.8347} - 0.0015 \beta_0^{1.835}\right)^{0.375} \tag{S36}$$

$$f_{B1} = 1.207 f_B \left(1 + 0.0001064 \beta_0^4 + 3.0\,10^{-7} \beta_0^5 + 0.068 \beta_0^{2.5}\right)^{0.3015} \tag{S37}$$

$$f_{B2} = 1.2254 f_B \left(1 + 0.054883 \beta_0^{2.2419}\right)^{0.38032} \tag{S38}$$

$$f_{B3} = f_B \frac{\frac{269.205}{\beta_0^{0.95686}} - 1.5}{\frac{230}{\beta_0^{0.9257}} - 1} \tag{S39}$$

$$f_{B4} = f_B \frac{0.0529478 \beta_0^{1.817} + 0.020928}{0.014925 \beta_0^{1.817} + 1} \tag{S40}$$

$$k = \left(1 + 0.217 \beta_0^{2.468}\right)^{0.1505} \tag{S41}$$

$$a = \left(1 + 0.0000079 \beta_0^{3.06}\right)^{0.1827} \tag{S42}$$

$$b = \frac{2.10315\,10^{-8} \beta_0^5 + 0.0586879 \beta_0^{2.335} + 1.0015}{0.04054 \beta_0^{2.4305} + 1} \tag{S43}$$

$$c = \frac{2\left(0.2211 \beta_0^2 + 1\right)^{0.9632}}{0.00029 \beta_0^3 + 0.227 \beta_0^{1.8233} + 1} \tag{S44}$$

$$d = 0.0013 \exp\left(-\frac{(\ln(\beta_0) - 14.771)^2}{8.3399^2}\right)\left(5000 e^{-0.127 \beta_0} + 1\right) + 1 \tag{S45}$$

$$g = \frac{0.6688 \beta_0^{0.5577}}{0.0041 \beta_0^{1.46} + 1} \tag{S46}$$

$$h = \frac{2\left(0.044 \beta_0^{2.217} + 1\right)^{0.29885}}{0.05955 \beta_0^{0.95936} + 1} \tag{S47}$$

$$j = \frac{0.0141 \beta_0^{2.586} + 0.00001658 \beta_0^{5.3936}}{3.68\,10^{-8} \beta_0^{6.4614} + 1} \tag{S48}$$

Fig. S6 compares the analytical approximation to Fokker-Planck simulations.

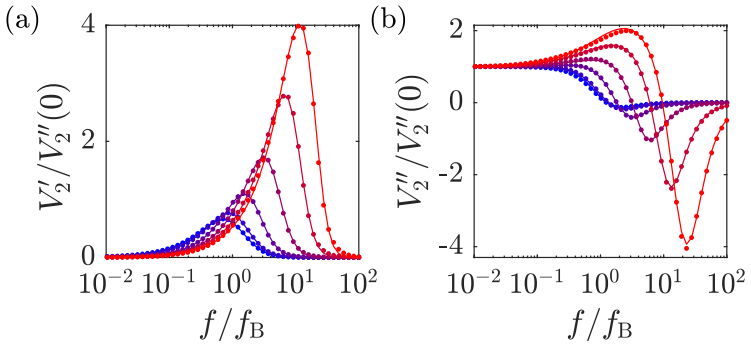

Fig. S6 Comparison between analytical approximation of the OM signal, Eqs. (S31)-(S45) (lines) and Fokker-Planck calculations with $\alpha = 0$ (points) for $\beta_0 = 0.99, 2.7, 7.2, 19, 52, 102$ (blue to red).

S6 Fitting optomagnetic data in the limiting cases

The size and magnetic moment can be obtianed in the limiting cases of field and frequencies for optomagnetic measurements as described in Fock *et al.* [6]

S6.1 Low-field behaviour vs. frequency

The size can determined from measurements of the low-field optomagnetic signal vs. frequency.

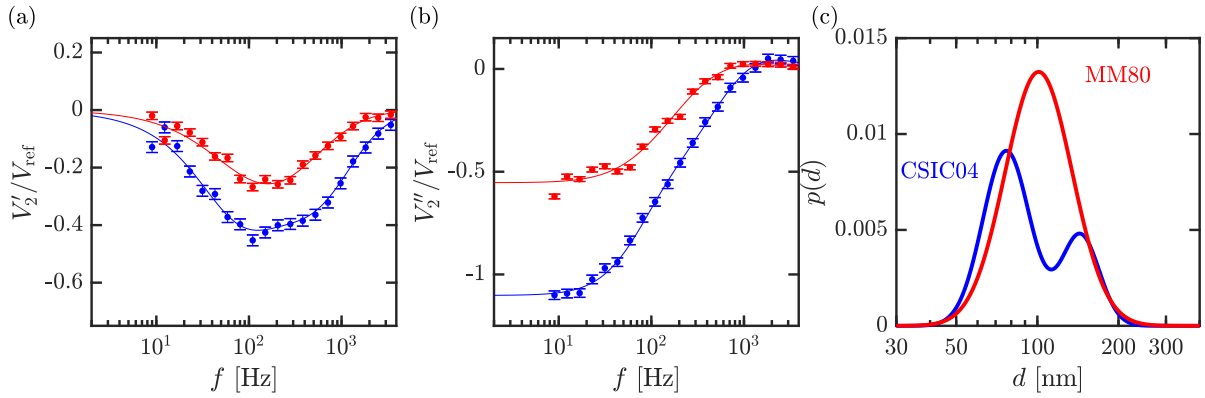

Fig. S7 Low-field (peak amplitude 0.35 mT) OM measurements of (a) $V_2'/V_{\rm ref}$ and (b) $V_2''/V_{\rm ref}$ vs. frequency for the NP1 (red) and NP2 (blue) samples (points). The error bars were calculated as the standard variation of the mean from five repeated measurements. The solid lines are fits to the low-field model assuming lognormal size distributions. (c) The size distributions obtained for the two particle systems.

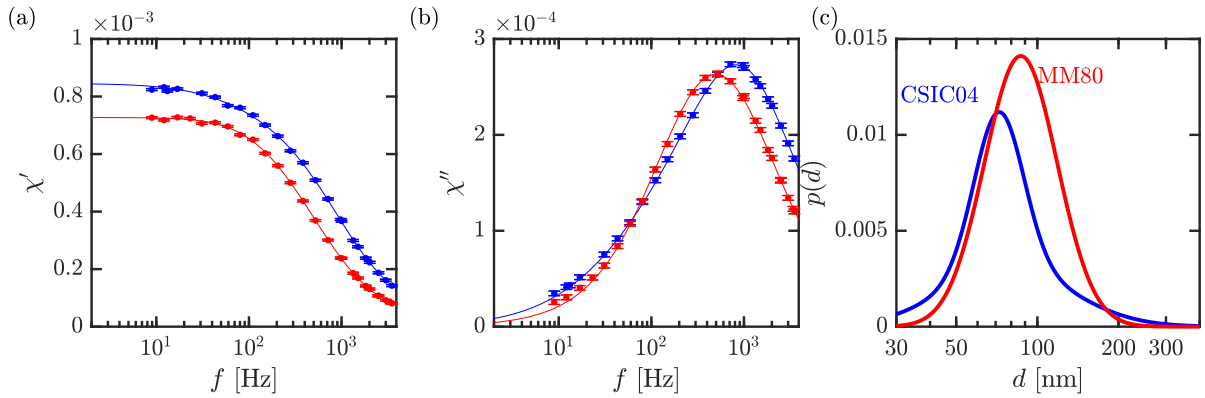

Fig. S8 Low-field (peak amplitude 0.35 mT) ACS measurements of (a) χ_1' and (b) χ_1'' vs. frequency for the NP1 (red) and NP2 (blue) samples (points). The solid lines are fits to the low-field Debye model assuming lognormal distributions of Brownian relaxation frequencies (hydrodynamic sizes). The error bars were adjusted to give the fit a reduced chi square value of 1. (c) The size distributions obtained for the two particle systems.

S6.2 Low-frequency vs. field behaviour

The magnetic moment can be determined from measurements of the low-frequency vs. field optomagnetic signal.

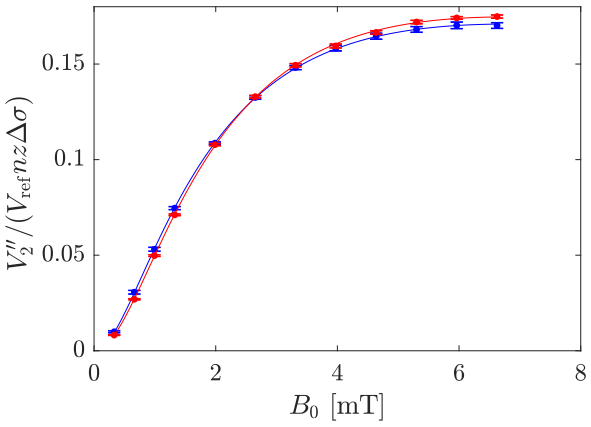

Fig. S9 Point are imaginary part of the low-frequency (equilibrium) optomagnetic measurements of NP1 (red) and NP2 (blue) samples. The lines are fits of the equilibrium model to the the second harmonic data (solid line and filled points). The plots were normalised by the signal strength $V_{\mathrm{ref}}nz\Delta\sigma$.

S7 Fitting to bivariate distribution

For a spectra measured at temperature T and with magnetic field strength H_0, the two-dimensional distribution in f_{B} and m, $p(f_{\mathrm{B}},m)\mathrm{d}\tau_{\mathrm{B}}\,\mathrm{d}m$, was first converted to a distribution in f_{B} and $\beta_0 = \mu_0 H_0 m/(k_{\mathrm{B}}T)$ as

$$p_{H_0}(f_{\mathrm{B}},\beta_0)\mathrm{d}f_{\mathrm{B}}\,\mathrm{d}\beta_0. \tag{S49}$$

Then, a one-dimensional discrete distribution was constructed,

$$\mathbf{p}^*_{H_0}(\{f_{\mathrm{B}},\beta_0\}) = p(f_{\mathrm{B}},m)\Delta f_{\mathrm{B}}\Delta\beta_0, \tag{S50}$$

describing the number fraction of particles with relaxation time between f_{B} and $f_{\mathrm{B}}+\Delta\tau_{\mathrm{B}}$ and with β_0 values between β_0 and $\beta_0+\Delta\beta_0$.

111 spectra for β_0-values chosen at equidistant logarithmic steps between 10^{-3} and 100 were calculated by solving the Fokker-Planck equation (Section 2.3) for 79 f/f_{B} values chosen at equidistant logarithmic steps between $3\cdot10^{-3}$ and 10^4.

Using linear interpolation, the spectral values were calculated at the N measurement frequencies for each of the 111 spectra with different β_0 values and with f_{B} ranging from 1 Hz to 10^5 Hz in 75 equidistant logarithmic steps. A total of 8325 spectra were obtained with the set of parameters $\{f_{\mathrm{B}},\beta_0\}$. The ACS spectra were arranged in a matrix, $\mathbf{S}_{\mathrm{ACS}}$ and the OM spectra were arranged in a matrix, $\mathbf{S}_{\mathrm{OM}}$, both with the size $N\times 8325$. The ACS and OM spectra measured at H_0 were then given by

$$\chi_1(H_0) = n\frac{k_{\mathrm{B}}T}{\mu_0 H_0^2}\mathbf{S}_{\mathrm{ACS}}\cdot\mathbf{p}^*_{H_0} + \chi_\infty \tag{S51}$$

$$\frac{\widetilde{V}_2(H_0)}{V_{\mathrm{ref}}} = -nz\frac{\widetilde{\Delta\sigma}}{\widetilde{m}^{n_\sigma/n_m}}\left(\frac{k_{\mathrm{B}}T}{\mu_0 H_0}\right)^{n_\sigma/n_m}\mathbf{S}_{\mathrm{OM}}\cdot\mathbf{p}^*_{H_0} \tag{S52}$$

where the matrix $\mathbf{S}_{\mathrm{ACS}}$ consisted of the spectra calculated using $\beta_0\overline{e_z}_{,1}$, whereas $\mathbf{S}_{\mathrm{OM}}$ consisted of the spectra calculated using $(\beta_0)^{n_\sigma/n_m}\overline{e_z^2}_{,2}$.

Increasing the spacing between magnetic moments and Brownian relaxation frequencies in $\mathbf{S}_{\mathrm{ACS}}$ and $\mathbf{S}_{\mathrm{OM}}$ did not change the result.

S8 Fits of data for the NP2 sample

The data for the NP2 sample was fitted using a bimodal bivariate distribution. In Fig. S10 the OM *and* ACS data were fitted, whereas in Fig. S11 only the ACS data was fitted.

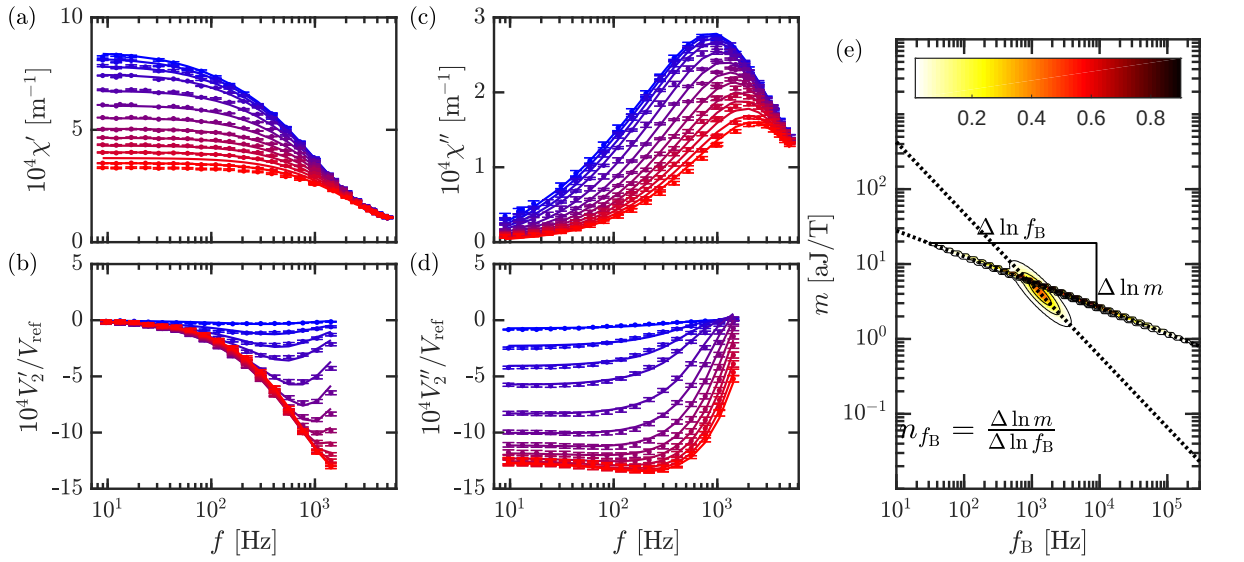

	$\mu_{f_{\rm B}}$ [kHz]	$\sigma_{f_{\rm B}}$	μ_m [aJ/T]	σ_m	ρ	$\frac{n_\sigma}{n_m}$	$\frac{nz\widetilde{\Delta\sigma}}{\tilde{m}^{n_\sigma/n_m}}$ [10^5]	n [10^{17}m^{-3}]	χ_∞	$n_{f_{\rm B}}$	$D_{\rm h}$ [nm]	$\overline{D_{\rm h}}$ [nm]
NP2	2.82(8)	1.60(1)	4.00(8)	0.550(8)	-1.00(1)	0.66(3)	-155.	1.82	0.039	-0.344(4)	56(1)	64(2)
-	1.336(1)	0.375(1)	4.02(6)	0.360(5)	-0.87(1)	6.1(1)	-0.00619	1.29	-	-0.95(2)	71.58(4)	72.14(4)

Fig. S10 Fit to NP2 ACS and OM data using a bimodal bivariate lognormal distribution. Panels (a) and (b) show the real and imaginary parts of the ACS data (points). Panels (c) and (d) show the real and imaginary parts of the OM data (points). The solid lines are the fit obtained from simultaneous analysis of all data to a bivariate distribution of Brownian relaxation frequencies and magnetic moments. The colours from blue to red correspond to increasing magnetic field amplitudes as given in the Methods section. Panel (e) shows the resulting bivariate distribution function. The distribution is normalised by its maximum value and the contour lines are at 0.01, 0.1, 0.3, 0.5, 0.7 and 0.9. The table shows the number-weighted fitting parameters.

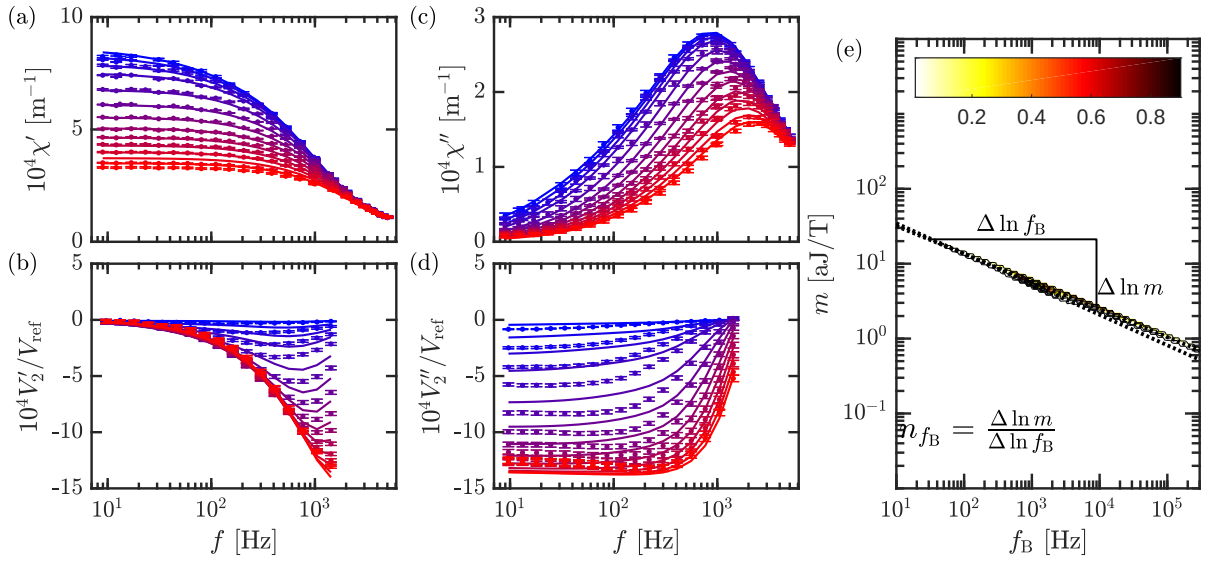

	$\mu_{f_{\rm B}}$ [kHz]	$\sigma_{f_{\rm B}}$	μ_m [aJ/T]	σ_m	ρ	$\frac{n_\sigma}{n_m}$	$\frac{nz\widetilde{\Delta\sigma}}{\widetilde{m}^{n_\sigma/n_m}}$ [10^5]	n [10^{17}m^{-3}]	χ_∞	$n_{f_{\rm B}}$	$D_{\rm h}$ [nm]	$\overline{D_{\rm h}}$ [nm]
NP2	6.1(6)	1.88(3)	3.0(2)	0.70(2)	-1.000(1)	2	-6.03	2.13	0.032	-0.371(8)	43(5)	53(5)
-	1.14(3)	0.44(3)	5.0(1)	0.18(3)	-1.000(7)	2	-22.6	1.23	-	-0.41(5)	75(2)	76(2)

Fig. S11 Fit to NP2 ACS data (only) using a bimodal bivariate lognormal distribution. Panels (a) and (c) show the real and imaginary parts of the ACS data (points). Panels (b) and (d) show the real and imaginary parts of the OM data (points). The solid lines are the fit obtained from simultaneous analysis of only the ACS data to a bivariate distribution of Brownian relaxation frequencies and magnetic moments. The colours from blue to red correspond to increasing field amplitudes as given in the Methods section. Panel (e) shows the resulting bivariate distribution function. The distribution is normalised by its maximum value and the contour lines are at 0.01, 0.1, 0.3, 0.5, 0.7 and 0.9. The table shows the number-weighted fitting parameters.

S9 Particle size distributions obtained by TEM

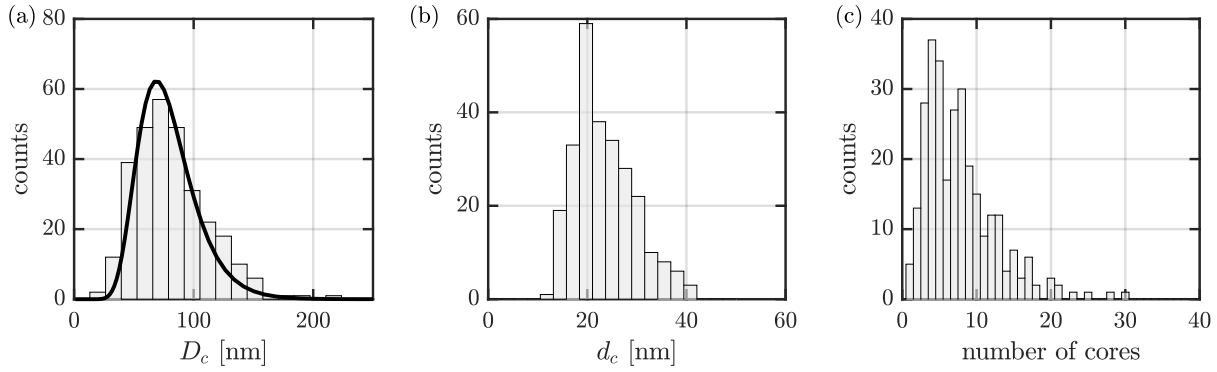

Fig. S12 Histogram of (a) particle size (b) core size and (c) number of cores per particle for the NP1 sample obtained from TEM images. The line in (a) is the number-weighted distribution obtained from the combined OM and ACS fit.

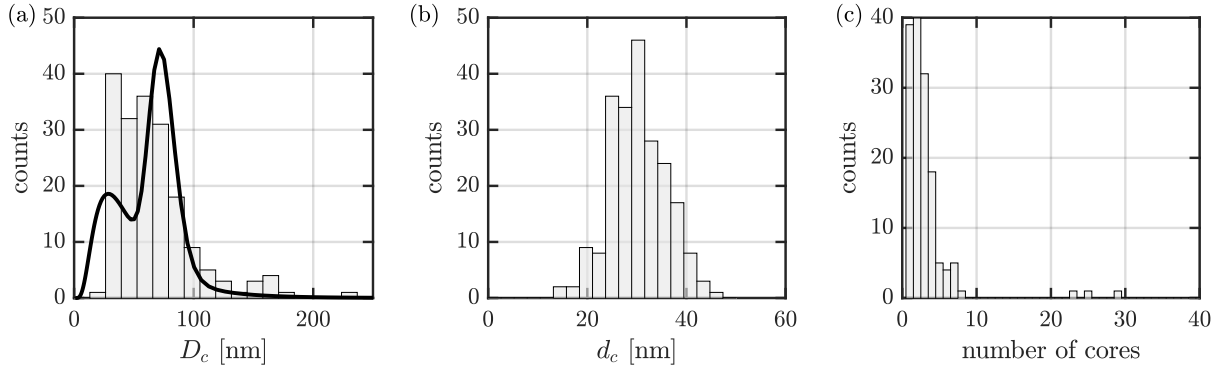

Fig. S13 Histogram of (a) particle size (b) core size and (c) number of cores per particle for the NP2 sample obtained from TEM images. The line in (a) is the number-weighted distribution obtained by fitting the ACS data (see Fig. S11).

S10 Matlab implementation of functions

S10.1 Fokker-Planck function

The section gives the implementation of the Fokker-Planck function in Matlab.

```
function [F] = FokkerPlanck( beta,gamma,f,L,N )
%% [F] = FokkerPlanck( beta,gamma,f,L,N )
%
% Please cite:
% Jeppe Fock, Christoph Balceris, Rocio Costo, Lunjie Zeng, Frank Ludwig, and Mikkel Fougt Hansen
% Nanoscale 2017
% "Field-dependent dynamic responses from dilute magnetic nanoparticle dispersions".
%
% == input ==
% beta: \mu_0 H m/(k_{\rm B} T)
% gamma:
% f: array of the reduced frequency - f/f_{\rm B}=\omega\tau_{\rm B} %
% L: truncation of L
% N: truncation of N
%
% == return ==
% F(i).A(l,n)=A_{l-1,n-1}
% F(i).B(l,n)=B_{l-1,n-1}
% F(i).cos= \cos \theta
% F(i).cos_square= \cos^2 \theta
% F(i).f=f
```

```
% F(i).resnorm: norm of residuals in the LSQR algorithm

xtmp=[];%initialize the vector for solutions
L2=[];
U2=[];
resnorm_lim=1e-13; %desired accuracy of the LSQR algorithm

for i=1:length(beta)
   F(i).f=f(i);
   F(i).beta=beta(i);
   F(i).gamma=gamma(i);

   % Write the systems of linear equations:
   [MM,fitI]=FokkerPlanckMatrix(beta(i),gamma(i),f(i),L,N );
   Y=-MM(2:end,1)*0.5; % MM is a matrix containing the linear equations
   MM=MM(2:end,2:end);

   if isempty(xtmp) % if first run, initailize starting point to default (all zeros.)
      xtmp=sparse(size(MM,2),1); %
   end

   % Solve the equation using the LSQR algoritme. Set maximum iteration
   % use the last results as starting point for LSQR
   [xtmp,flag,resnorm,iter,resvec]=lsqr(MM,Y,resnorm_lim,1000000,[],[],xtmp);

   x=sparse(L*N*2,1);
   x(fitI)=[0.5;xtmp];

   % Formating returns:
   Aret=@(l,n) x((l*N+n)*2+1);
   Bret=@(l,n) x((l*N+n)*2+2);

   F(i).cos=2/3*(Aret(1,1:N-1)+Bret(1,1:N-1)*1i);
   F(i).cos_square=[4/15*(Aret(2,1:N-1)+1i*Bret(2,1:N-1)); 4/15*Aret(2,0)+1/3];
   F(i).resnorm=resnorm;
   F(i).flag=flag;
end
end

function [ M, fitI] = FokkerPlanckMatrix( beta,gamma,f,L,N )
%[ M, fitI] = FokkerPlanckMatrix3( beta,gamma,f,L,N )
%
% make matrix of linear equations.

kroneckerDelta =@(x) x==0;
% make a diagonal matrix with the row/column "(l*N+n)*2" corresponding to A_{l,n}
% and "(l*N+n)*2" corresponding to B_{l,n}:

% A_{l,n}=X((l*N+n)*2+2*N+3)
% B_{l,n}=X((l*N+n)*2+1+2*N+3)
X = diag(sparse(ones(1,2*L*N)));
X=[sparse(2*L*N,2*N+2) X];

%set the element zero if it is defined zero. The element will later be
%removed from the equations.
%even and odd
X(:,(0*N+(1:N-1))*2+2*N+3)=0;%A(0,n)=0 ,for n>=1
X(:,(0*N+(0:N-1))*2+1+2*N+3)=0;%B(0,n)=0,for n>=0
X(:,((0:L-1)*N+0)*2+1+2*N+3)=0;%B(l,0)=0

% calculate only even numbers
index=bsxfun(@plus,(0:2:L-1)*N,(1:2:N-1)');%B(l,n)=0 for l even n odd

X(:,index(:)*2+1+2*N+3)=0; %B(l,n)=0 for l even n odd
X(:,index(:)*2+2*N+3)=0; %A(l,n)=0 for l even n odd

index=bsxfun(@plus,(1:2:L-1)*N,(0:2:N-1)');%for l odd n even
```

```
X(:,index(:)*2+1+2*N+3)=0; %B(l,n)=0 for l odd n even
X(:,index(:)*2+2*N+3)=0; %A(l,n)=0 for l odd n even

   function x=fA(l,n) % function to convert from matrix A_{l,n} to the vector X
     x=X(:,(l*N+n)*2+2*N+3);

   end
   function x=fB(l,n) % function to convert from matrix B_{l,n} to the vector X
        x=X(:,(l*N+n)*2+1+2*N+3);
   end

xtmp=[];%initialize the vector for solutions
M=sparse(2*L*N,(L-2)*((N-2)+1));
M(:,1)=fA(0,0); %A_{0,0}=1 , the only non-homogeneous equation
% Write the systems of linear equations:

for l=1:L-3
    n=(2-mod(l,2)):2:N-3;
      M(:,((l*N+n)*2+1))=-fA(l,n)+...
         beta/2*(1/(2*l-1)*(bsxfun(@times,(1+kroneckerDelta(1-n)),fA(l-1,n-1))+fA(l-1,n+1))-...
         1/(2*l+3)*(bsxfun(@times,(1+kroneckerDelta(1-n)),fA(l+1,n-1))+fA(l+1,n+1)))+...
         gamma/4*(...
         (l-1)/((2*l-3)*(2*l-1))*(bsxfun(@times,(2+kroneckerDelta(1-n)),fA(l-2,n))+ ...
           bsxfun(@times,(1+kroneckerDelta(2-n)),fA(l-2,n-2))+fA(l-2,n+2))+...
         1/((2*l+3)*(2*l-1))*(bsxfun(@times,(2+kroneckerDelta(1-n)),fA(l,n))+ ...
           bsxfun(@times,(1+kroneckerDelta(2-n)),fA(l,n-2))+fA(l,n+2))-...
         (l+2)/((2*l+5)*(2*l+3))*(bsxfun(@times,(2+kroneckerDelta(1-n)),fA(l+2,n))+ ...
           bsxfun(@times,(1+kroneckerDelta(2-n)),fA(l+2,n-2))+fA(l+2,n+2)))-...
         bsxfun(@times,n*2*f/(l*(l+1)),fB(l,n));
         M(:,((l*N+n)*2+2))=-fB(l,n)+...
         beta/2*(1/(2*l-1)*(fB(l-1,n-1)+fB(l-1,n+1))-...
         1/(2*l+3)*(fB(l+1,n-1)+fB(l+1,n+1)))+...
         gamma/4*(...
         (l-1)/((2*l-3)*(2*l-1))*(bsxfun(@times,(2-kroneckerDelta(1-n)),fB(l-2,n))+fB(l-2,n-2)+fB(l-2,n+2))+...
         1/((2*l+3)*(2*l-1))*(bsxfun(@times,(2-kroneckerDelta(1-n)),fB(l,n))+fB(l,n-2)+fB(l,n+2))-...
         (l+2)/((2*l+5)*(2*l+3))*(bsxfun(@times,(2-kroneckerDelta(1-n)),fB(l+2,n))+fB(l+2,n-2)+fB(l+2,n+2)))+...
         bsxfun(@times,n*2*f/(l*(l+1)),fA(l,n));
   if mod(l,2) % Skip odd values
      continue
   end
   n=0;
   M(:,((l*N+n)*2))= -fA(l,0)+...
      beta/2*(1/(2*l-1)*(fA(l-1,1))-...
      1/(2*l+3)*(fA(l+1,1)))+...
      gamma/4*(...
      (l-1)/((2*l-3)*(2*l-1))*(2*fA(l-2,0)+fA(l-2,2))+...
      1/((2*l+3)*(2*l-1))*(2*fA(l,0)+fA(l,2))-...
      (l+2)/((2*l+5)*(2*l+3))*(2*fA(l+2,0)+fA(l+2,2)));
end
   KeepLines=find(sum(abs(M),1)~=0);% Find non-empty equations
   M=M(:,KeepLines);%reduce matrix
   fitI=find(sum(abs(M),2)~=0); %only fit varibles which are not defined nonzero.
   M=M(fitI,:)';
end
```

S10.2 Analytical OM function

The section gives the implementation of the analytical OM function in Matlab.

```
function V2 = NanalyticV2(f,beta)
%% V2 = NanalyticV2(f,beta)
%
% calculate the analytical OM response valid for beta values <300
%
% f is the frequency normalized with f_B
% beta = m B_0/(k_B T)
```

```
% V2=V2'+1i V2'': The complex optomagnetic second harmonic response.
%
% Please cite:
% Jeppe Fock, Christoph Balceris, Rocio Costo, Lunjie Zeng, Frank Ludwig, and Mikkel Fougt Hansen
% Nanoscale 2017
% "Field-dependent dynamic responses from dilute magnetic nanoparticle dispersions".
%

   f0 = (beta.^( 1.8350).*(-0.0016)+beta.^1.8347.*(0.0512)+1).^(0.375).*1.22475;
   V20 = beta.^2./(beta.*(-1.56e-2)+beta.^1.8036.*0.1051+beta.^2.7939.*7.298e-3+1).^0.99666./45);
   fB1 = (beta.^4.*1.064e-4+beta.^5.*3.0e-7+beta.^(5/2).*(1.7e1./2.5e2)+1).^3.015e-1.*1.207;
   fB2 = (beta.^2.2419.*5.4883e-2+1).^0.38032.*1.2254;
   fB3 = (1./beta.^9.5686e-1.*2.69205e2-3./2)./(1./beta.^0.9257.*2.3e2-1);
   fB4 = (beta.^1.817.*5.294784e-2+2.0928e-2)./(beta.^1.817.*1.4925e-2+1);
   k = (beta.^(2.468).*(2.17e2./1e3)+1).^1.505e-1;
   a = (beta.^(3.06).*7.9e-6+1).^0.1827;
   b = (beta.^5.*2.10315e-8+beta.^( 2.335).*5.86879e-2+1.0015)./(beta.^2.4305.*4.054e-2+1);
   c = ((beta.^2.*0.2211+1).^(0.9632).*2)./(beta.^3.*2.9e-4+beta.^1.8233.*(0.227)+1);
   d = exp((log(beta/2.6e+06)).^2.*(-0.1199^2)).*(exp(beta.*( -0.1270)).*5e3+1).*1.3e-3+1;
   g = (beta.^5.577e-1.*(0.6688))./(beta.^(7.3e1./5.0e1).*4.1e-3+1);
   h = ((beta.^2.217.*(1.1e1./2.5e2)+1.0).^0.29885.*2)./(beta.^9.5936e-1.*5.955e-2+1);
   j = (beta.^2.586.*1.41e-2+beta.^5.3936.*1.658e-5)./(beta.^6.4614.*3.68e-8+1);

   imagV2
       =-((f./f0).^2-1).*((f./fB2).^h+1).^(d.*-2).*(f./fB3+1).^g.*((f./f0+1).^2./(f./fB4+1).^2).^j;
   realV2 =2.^a.*k.*(f./fB1).^b.*((f./fB1).^c+1).^(a.*-2);
   V2=(realV2+1i*imagV2).*V20;
end
```

S10.3 Analytical ACS function

The section gives the implementation of the analytical ACS function in Matlab.

```
function Chi = NanalyticACS(f,beta)
%% Chi = NanalyticACS(f,beta)
%
% f is the frequency normalized with f_B
% beta = m B_0/(k_B T)
% Chi=Chi'-1i Chi'': The complex susceptibility.
%
% Please cite:
% Jeppe Fock, Christoph Balceris, Rocio Costo, Lunjie Zeng, Frank Ludwig, and Mikkel Fougt Hansen
% Nanoscale 2017
% "Field-dependent dynamic responses from dilute magnetic nanoparticle dispersions".
%

   chi10 = (1./(1-beta.^1.*2.47e-2+beta.^(1.7).*(0.135)+ beta.^(2.7).*2.71e-2)).^(0.37);
    fB1 = (beta.^2.*(0.144)+1).^(0.3950);
    fB2 = (beta.^2.*9.08e-2+1.0).^(0.48);
    a = (beta.^(2.2).*2.52e-2)./(beta.^(1.4).*(0.2390)+beta.^(2.3).*( 0.0144)+1)+1;
    b = (beta.^(2.5).*(-2.14e-3)).(beta.^( 1.45).*7.37e-2+beta.^(2.45).*6.79e-3+1)+1;
    c = (beta.^(2.2).*2.01e-2)./(beta.^(1.4).*(0.16)+beta.^(2.1).*2.29e-2+1)+1;

    realChi = chi10.*(f.^2.*1./fB1.^2+1).^(-a);
    imagChi = (chi10.*((f.*c)./fB2).^b)./(f.^2./fB2.^2+1);
    Chi = realChi + 1i*imagChi;
end
```

S11 Higher harmonics

The higher harmonics are also obtained from the Fokker-Planck calculations and can be used to characterise magnetic nanoparticles. Martens *et al.* [8] used the ratio between higher harmonics to characterise magnetic nanoparticles and found that they needed to use a distribution of particle sizes to describe AC susceptibility data properly. They solved the Fokker-Planck equation using the ode15s routine in MATLAB®. Figure S14 shows that it is possible to reproduce their curves using the solution to the Fokker-Planck equation presented in this paper.

The p'th harmonic is calculated using only a single moment and consequently a constant β_0 as

$$\chi_p(f) = \frac{3\chi_0}{\beta_0} \int \overline{e_{z,p}}(f/f_\mathrm{B}, \beta_0) p(f_\mathrm{B}) \mathrm{d}f_\mathrm{B} \tag{S53}$$

where the distribution is either monodisperse ($p(f_\mathrm{B}) = \delta(f_\mathrm{B} - f_{\mathrm{B}0})$, where δ is the delta function) or given as a Gamma distribution of the hydrodynamic radius, R as

$$p(f_\mathrm{B})\mathrm{d}f_\mathrm{B} = \frac{1}{R_0\Gamma(\beta+1)} \left(\frac{R(f_\mathrm{B})}{R_0}\right)^\beta \exp(-R(f_\mathrm{B})/R_0)\mathrm{d}f_\mathrm{B} \tag{S54}$$

$$R(f_\mathrm{B}) = \left(\frac{k_\mathrm{B}T}{\pi^2\eta f_\mathrm{B}}\right)^{1/3} \tag{S55}$$

with the parameters R_0 and β defined in Martens *et al.*[8]

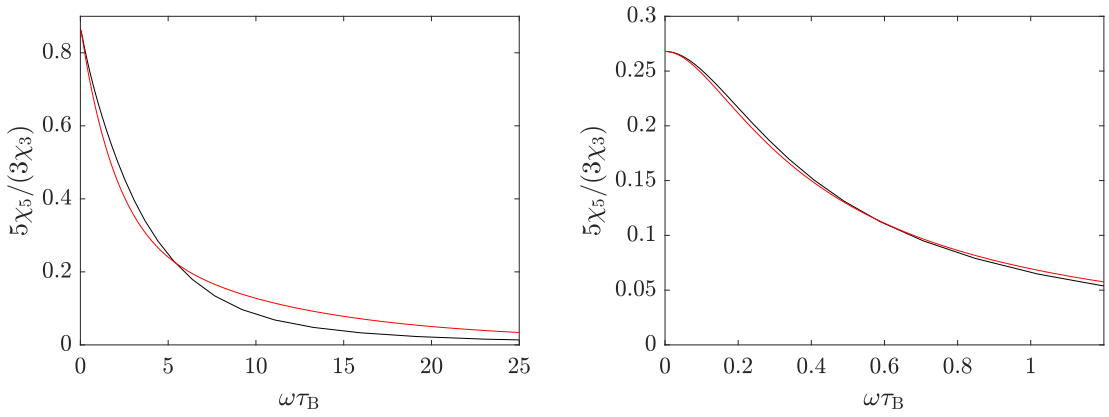

Fig. S14 Reproduced figure 2 and 3 from Martens *et al.*[8]. Ratio of the fifth and third harmonic of the AC susceptibility for 100 nm particles (left) and 40 nm particles (right). Black curves are calculated using monodisperse distributions and red using the distributions defined in Martens *et al.*[8]

References

1 S. H. Koenig, *Biopolymers*, 1975, **14**, 2421–2423.

2 D. B. Reeves and J. B. Weaver, *J. Appl. Phys.*, 2012, **112**, 1–6.

3 J. L. García-Palacios and F. J. Lázaro, *Phys. Rev. B*, 1998, **58**, 14937–14958.

4 M. Raible and A. Engel, *Appl. Organomet. Chem.*, 2004, **18**, 536–541.

5 C. Aron, D. G. Barci, L. F. Cugliandolo, Z. G. Arenas and G. S. Lozano, *J. Stat. Mech. Theory Exp.*, 2014, **2014**, P09008.

6 J. Fock, C. Jonasson, C. Johansson and M. F. Hansen, *Phys. Chem. Chem. Phys.*, 2017, **19**, 8802–8814.

7 T. Yoshida and K. Enpuku, *Jpn. J. Appl. Phys.*, 2009, **48**, 127002.

8 M. A. Martens, R. J. Deissler, Y. Wu, L. Bauer, Z. Yao, R. Brown and M. Griswold, *Med. Phys.*, 2013, **40**, 022303.